Prediction of compressive characteristic of hat section high-strength steel frame taking the Bauschinger effect into account

Kenji Takada [a], Masaki Matsuo [a], Kenichiro Fukagawa [a], Kentaro Sato [b], Pierre Farahat [c] , Lamine Diallo [d] , Yangwook Choi [e] , Anwer Yasin [c]

[a] Honda R&D Co., Ltd. 4630 Shimotakanezawa, Haga-machi, Haga-gun, Tochigi, 321-3393 Japan
[b] JFE Steel Corporation, 1 Kawasaki-cho, Chuo-ku,Chiba 260-0835, Japan
[c] Dassault Systèmes K.K., ThinkPark Tower, 2-1-1 Osaki, Shinagawa-ku, 141-6020 Tokyo, Japan
[d] Dassault Systemes Canada Inc. 393 St-Jacques Street West, Suite 300 Montreal, QC H2Y 1N9 | Canada
[e] Dassault Systemes Simulia Corp, 1301 Atwood Ave., Suite 101W, Johnston, RI 02919, United States

***Abstract**: In recent years, the usage of high-strength steel is increasing in order to improve the rate of body weight reduction and the safety performance of a vehicle from crash. The Bauschinger effect is generally strong in high-strength steel sheets. Material properties used in crash analysis is conventionally treated as isotropic hardening material. However, the analysis results such as average loading and buckling wavelength from analysis deviates with those from tests, which is observed in some axial collapse problems of hat section frame that is composed of high-strength steel sheet. When axial collapse occurs in the hat cross section frame, buckling occurs along with a frame ridge rolling. The Bauschinger effect will occur in the steel sheet at both front and back surfaces as the rolling progresses. In order to perform the axial collapse analysis considering the Bauschinger effect, performing high-strength steel sheet tension-compression tests and calibrating the parameters of the Bauschinger effect are necessary. In this study, a correlation tool has been developed to perform the correlation process by using Isight and Abaqus. It is confirmed that the analysis results fit test results in good precision in both Chaboche and modified ANK models using the parameters generated by the tool.*

***Keywords**: Material models, the Bauschinger effect, Chaboche, Hardening, Crash analysis.*

1. Introduction

The use of high-strength steels in automobile body structures has been considered an efficient solution because of the lower cost of volume production in the automotive industry. With the improvement of the formability of high-strength steels by optimizing the metallic microstructure, the range of application of high-strength steels has been expanding in automobile body structures. Recently, advanced high-strength steels with strengths from 980MPa to 1500MPa used in automotive bodies have played a crucial role in crash safety performance. To design and manufacture automotive parts from high-strength steels, simulation has become an indispensable tool for the prediction of energy absorption during crash of a vehicle.
The Bauschinger effect has been studied in plastic forming field, and there are many models such as Armstrong and Frederick model, Chaboche model, ANK model, ZANG model and etc. have been proposed for representing the Bauschinger effect. On the other hand, the Bauschinger effect

is not considered in crash analysis fields. In many recent study of static crash analysis of hat-section problems, the amount of energy absorption was found higher than the ones from the tests. For studying the Bauschinger effect in crash analysis, author (1) has performed many tension-compression tests since 1999 but the author did not always satisfied with the results because of occurrence of the buckling in the compression period. After adding buckling prevention back plates to the tesreg in 2012, additional tests were performed by JFE. As the result, we are succeeded to obtain test results with high accuracy for tension-compression test using high-strength steel materials. We studied on FEA analysis to reproduce the characteristics of the tension-compression model. For the first, using the kinematic hardening component of Abaqus, we performed calibration of material parameters for the first back-stress of Chaboche model. And then we performed static crash analysis of both hat section frames and hexagonal section frames using those parameters. It was found that the analysis results were reproducing test results with good accuracy. During the study, we developed a tool for calibrating the material properties of Chaboche and modified ANK models up to the second back-stress quickly. From analysis results, it was found that modified ANK model was more effective for obtaining results with high accuracy in tension-compression crash analysis.

2. Axial crush tests and calculations

The axial crush tests and simulations with hat section and hexagonal section frame were performed to investigate the energy absorptions of each frame. The steel grades used in this test were 590MPa and 780MPa grade. Figure 1 shows the specification of the hat section and hexagonal section frames. The hat section is 60mm x 60mm cross section, 20mm flange width, and thickness t=1.6mm while the hexagonal section is 34.64mm sides, 20mm flange width, and thickness t=1.6mm. The width-to-thickness ratios (C/t) of the hat section and hexagonal section were 37.5 and 21.7, respectively. Therefore, it was supposed that these frames had plastic buckling. The amsler tests were performed with a constant velocity of 1mm/sec. The Table 1 shows the material properties for two classes of steels.

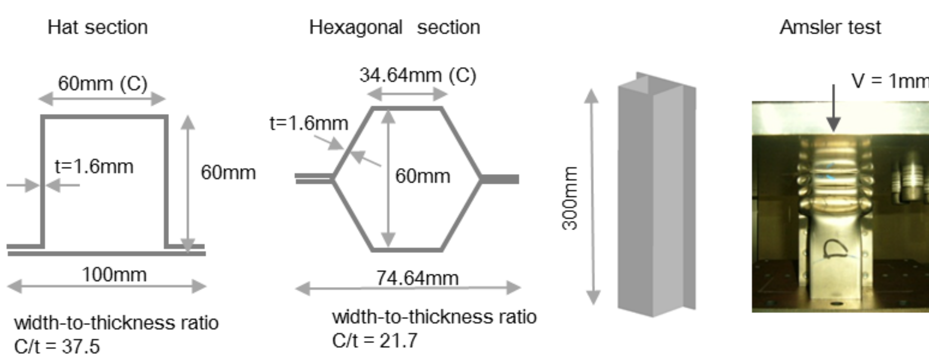

Figure 1. Dimension of the hat section and hexagonal section

Table 1. Material properties for two classes of steels

	Thickness(mm)	YS (MPa)	TS (MPa)	n-value	direction
590MPa	1.6	370	568	0.151	0°
780MPa	1.6	463	752	0.114	0°

2.1 FEA models

The hat section frame of 60mm x 60mm cross section and length L=300mm with thickness t=1.6mm was used. Furthermore, the hexagonal section frame of one side a=34.64mm and length L=300mm with thickness t=1.6mm was also considered in this study shown in Figure 2. The fixed boundary condition was applied at the bottom end of both frames. For the top end of both frames five degrees of freedom (u_y , u_z , θ_x , θ_y , θ_z) were fixed to generate the plastic buckling in the middle of frames. The enforced velocity was applied at the top end of the frames. FEM models were modeled with 4-node shell element using Abaqus element type S4.

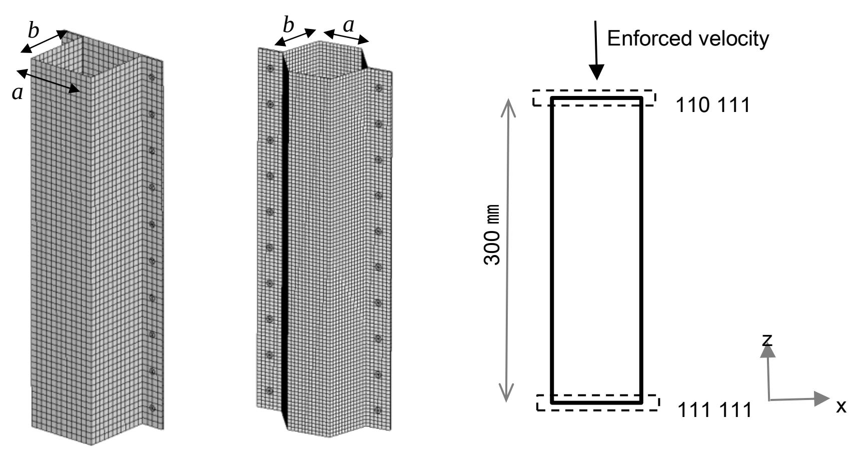

Figure 2. Dimension of the hat section and hexagonal section of FEA

2.2 Determination of mesh pitch

In this study, the element length (mesh pitch) of a 4-node shell element was decided based on the length of the plastic buckling folding wave. There are several equations to calculate the plastic folding wave length of thin-walled columns. In this study, Abramowicz and Wierzbicki equation was applied as shown in Equation 1 (Wierzbicki, Recke, Abramowicz and Gholami, 1994).

$$H = t^{1/3} b^{2/3} \tag{1}$$

$$C = \frac{1}{2}(a + b) \tag{2}$$

where H is a quarter folding length, t is the thickness, C is the mean value of two sides (a,b) of the cross section.

Figure 3 shows the plastic folding wave of thin-walled prismatic frame. It is supposed that plastic folding wave shows a cubic curve in the cut section (Wierzbicki and Abramowicz, 1989). Therefore, it is assumed that the total number of the divisions to predict the folding wave correctly is 7 or 8. According the Equation 1, the length of plastic folding wave of hat section frame and hexagonal section frame are 35.2mm and 24.3 mm respectively. Consequently, in the FEA, it was defined that the mesh pitch of hat section was 5mm and hexagonal section was 2.88mm as shown in Table 2.

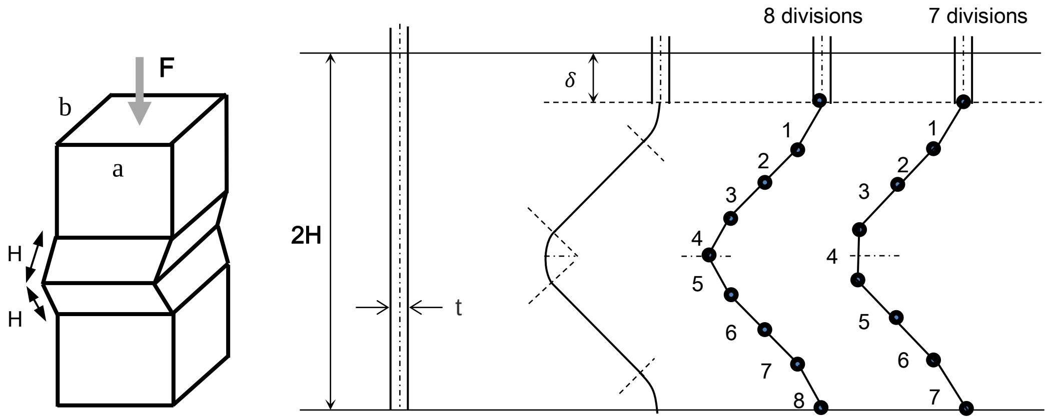

Figure 3. Relationship between plastic folding wave and mesh pitch

Table 2. Element length of FEA models

	Length of a plastic folding wave, 2H	Element length
Hat section	35.2mm	5mm
Hexagonal section	24.3mm	2.88mm

2.3 Stress-strain curves

In FEA, the swift equation shown in Equation (3) is applied to express the stress-strain relation after uniform elongation (n-value) (Datsko, 1966).

$$\sigma = \sigma_0 \left(\varepsilon_0 + \bar{\varepsilon}^{pl} \right)^n \tag{3}$$

where σ_0 , ε_0 and n are the strength coefficient, yield strain and strain hardening exponent respectively. Figure 4 shows the true stress-strain curves for two classes of steels used in FEA.

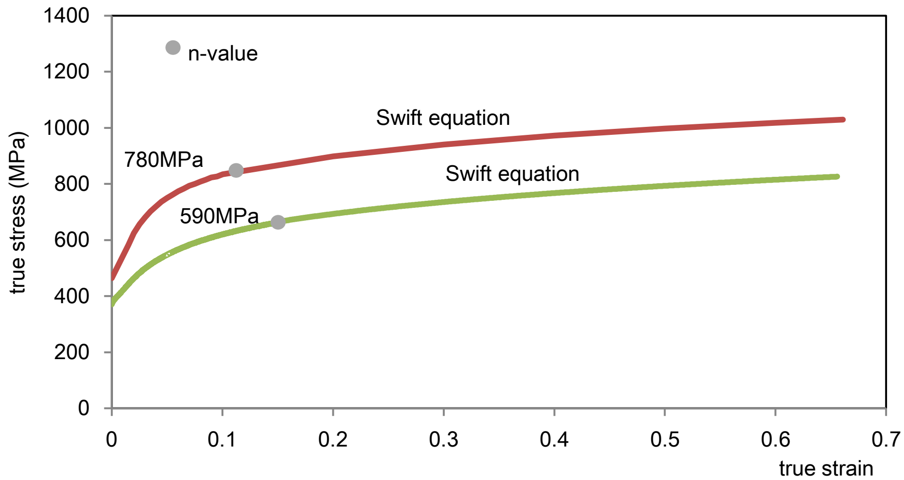

Figure 4. Dimension of the hat section and hexagonal section of FEA

2.4 Axial crush calculation

Figure 5 shows the force-stroke and energy-stroke curves of the hat section frames and the hexagonal section frame obtained by the experiment and Abaqus. In Figure 5 (a), (b), the energy absorption of 590MPa and 780MPa grade from FEA were larger than test results. Meanwhile, in the case of hexagonal section frames shown in Figure 5 (c), (d), the energy absorption of 590MPa and 780MPa grade calculated by FEA were much larger than test results. In the FEA, the isotropic hardening material model of Abaqus was applied. The 590MPa and 780MPa grade are high-strength steels. It was supposed that both steels had to consider the Bauschinger effect.

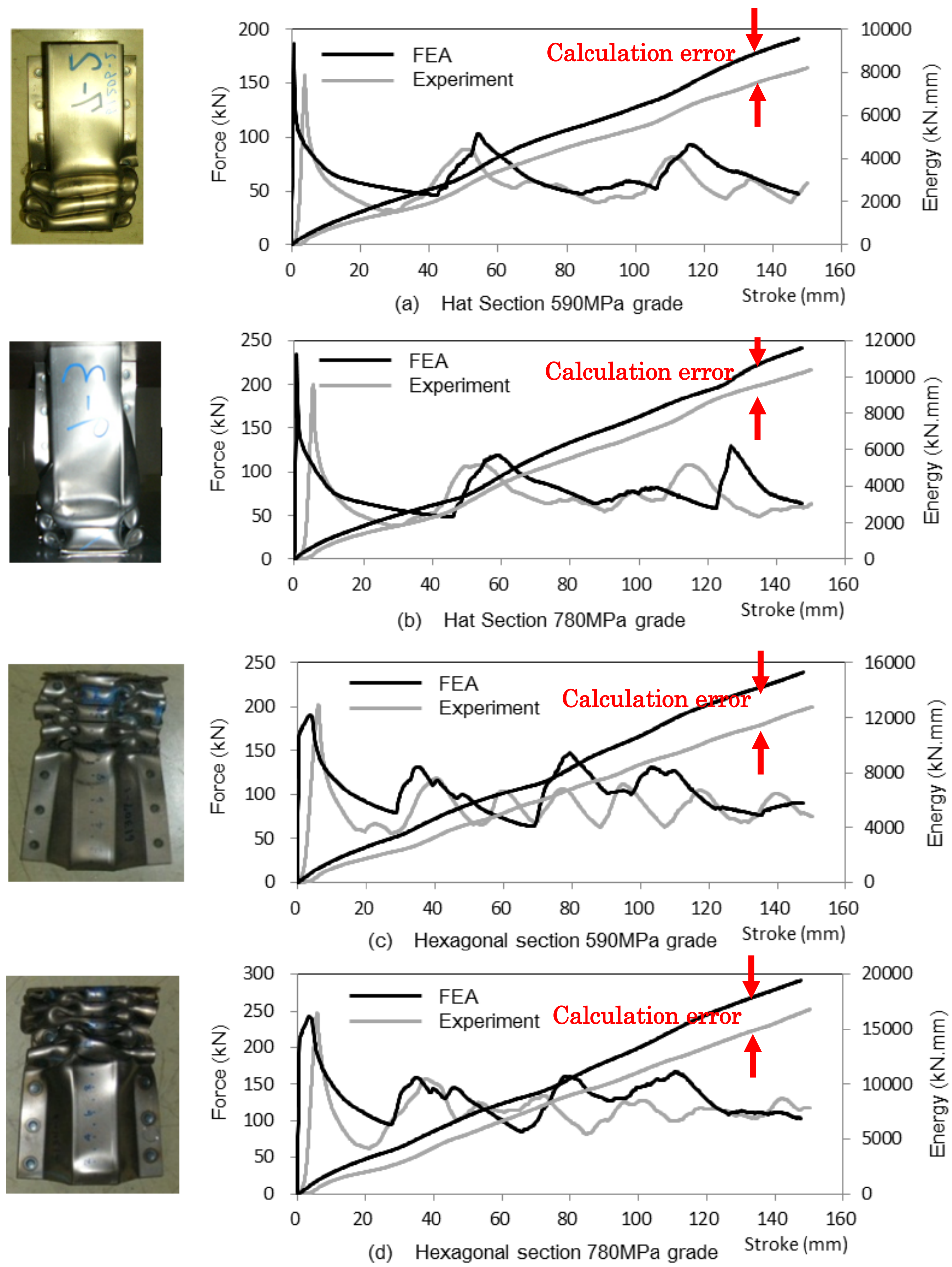

Figure 5. Force-stroke and energy-stroke curves of the hat section frames

3. Modeling of the Bauschinger effect

3.1 Moving hinge lines in deformation mechanism

In this study, it was considered the reason why energy absorptions of 590MPa and 780MPa grade frame had calculation errors. Figure 6 shows the deformation mechanism of thin-walled prismatic frame. The deformation of thin-walled prismatic frame is progressed by the folding of the wall. Initial hinge line (1-C-2) moves to point B (1-B-2) by the folding of wall, which is named as moving hinge line. In the initial condition, the point B is on the middle of the wall. However, when the initial hinge line (1-C-2) moves to point B, the tensile stress occurs at the surface of the point B (reverse face of point B becomes compression). In the next step, when the moving hinge line (1-B-2) moves to point A (1-A-2), the compression stress occurs at the surface of point B (on the surface of the other side point B becomes tensile). In other words, in the case of axial crush problem of thin-walled frame, along with the moving hinge line the material experiences cyclic loading. Therefore, the Bauschinger effect should be considered.

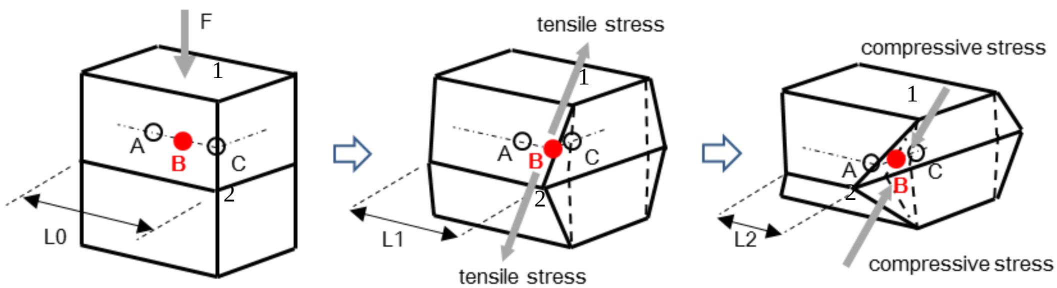

Figure 6. Moving hinge line in deformation mechanism

Figure 7 shows the energy absorption of point B. If the material model is for isotropic hardening, the energy absorption of point B is expressed in Figure 7 (a). In contrast to that if the material model is for complex hardening (the Bauschinger effect), the energy absorption is expressed in Figure 7 (b). Hence, the energy absorption of isotropic hardening is larger than complex hardening. It is supposed that the Bauschinger effect is the reason why energy absorptions of 590MPa and 780MPa grade frame had calculation errors.

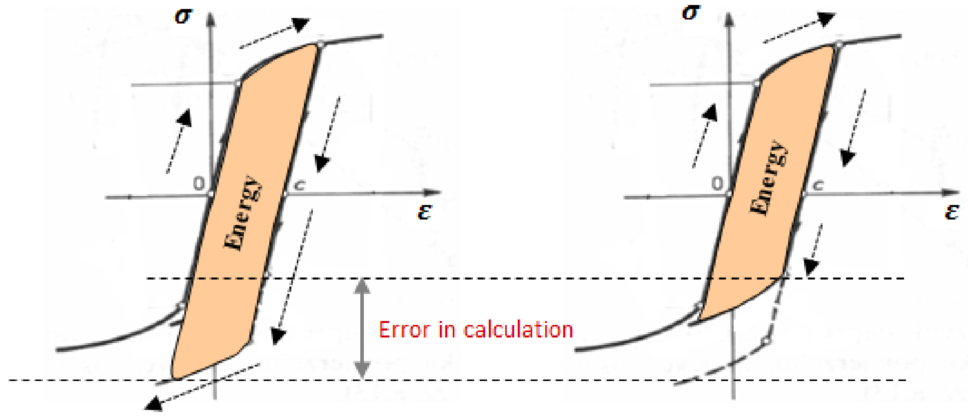

(a) Isotropic hardening (b) Complex hardening (Bauschnger effect)

Figure 7. Energy absorption of isotropic and complex hardening

3.2 Tensile and compression tests

Tensile and compression test was performed to measure the Bauschinger effect of standard high-strength steels, which was performed by JFE steel. Figure 8 shows the measuring system for the Bauschinger effect. Basically, in the tension and compression test, buckling of the test specimen occurs in the compression state. In this system, the buckling prevention back plate was used to prevent the buckling. High quality oil was added between buckling prevention back plate and test specimen to decrease the friction.

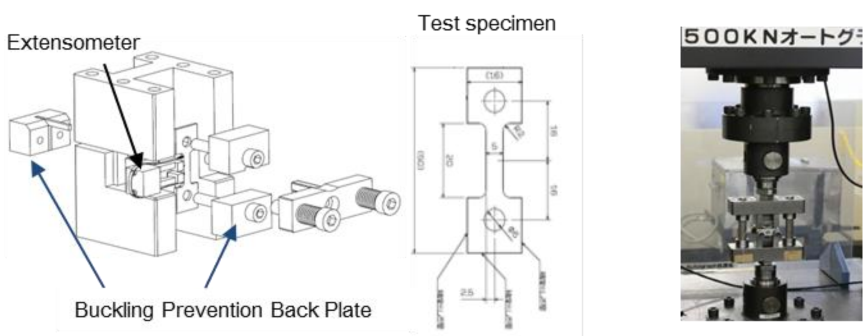

Figure 8. Tensile and compression test with buckling prevention back plate

Figure 9 shows the tensile and compression curves of 590MPa and 780MPa grades obtained by tests. In the case that FEA supposes the stress-strain curve as isotropic hardening; the dotted lines are stress-strain curves of FEA in compression state. Its flow stress is larger than test and Young's modulus is also larger than test.

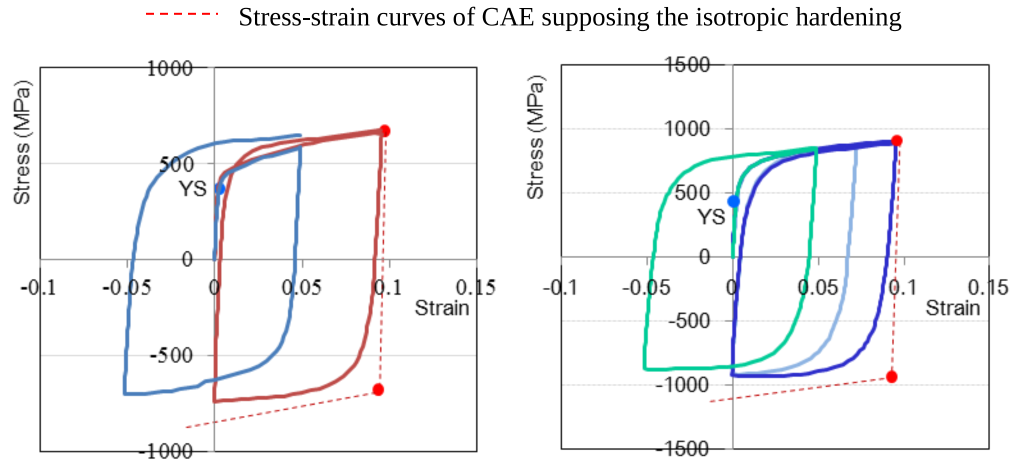

(a) 590MPa grade (b) 780MPa grade

Figure 9. Tensile and compression curves of 590MPa and 780MPa grade

3.3 Numerical models for the Bauschinger effect

Some materials show that the yield stress obtained in the reloading or reversed directional loading is substantially less than the yield stress obtained in the original loading direction. It has been observed in polycrystalline metals as well as single crystal metals. The behavior is called as the Bauschinger effect which can be described by the kinematic hardening model. Some materials show that the yield stress for the cyclic loading does not reach the first yield which we call permanent softening. These behaviors can be explained by the dislocation pile up and tangles due to the previous loading cycles and can also be described by Armstrong-Frederick type backstress evolution model for the transition of the yield surface (Armstrong and Frederick, 1966). The understanding of the Bauschinger effect and implementation of the effect in the plastic deformation are important to predict the material deformation correctly. There are many models that can describe the Bauschinger effect: Chaboche (Chaboche, 1986), modified Chaboche (Chaboche, 1989), ANK (Chun et al, 2002), Frederic-Armstrong (Armstrong and Frederick, 1966), etc. These models are believed to be the most suitable algorithms for describing the behaviors of high-tension steels.

The underlined material behavior cannot be explained by isotropic hardening model; hence, kinematic hardening model was introduced

$$F = f(\boldsymbol{\sigma}-\boldsymbol{\alpha})+\sigma^0 = f(\boldsymbol{\sigma}-\boldsymbol{\alpha})+\sigma_0 + R \quad (4)$$

where $\boldsymbol{\sigma}$ is stress tensor, $\boldsymbol{\alpha}$ is backstress tensor, and R is the isotropic hardening part. The backstress $\boldsymbol{\alpha}$ can be considered to be the sum of multiple backstress component tensors

$$\boldsymbol{\alpha} = \sum_i \boldsymbol{\alpha}_i \ . \quad (5)$$

Each component of the backstress is assumed to evolve independently as described by Armstrong-Frederick type backstress evolution *(Ref)*:

$$\dot{\boldsymbol{\alpha}} = \frac{C_i}{\sigma^0}(\boldsymbol{\sigma}-\boldsymbol{\alpha})\dot{\bar{\varepsilon}}^{pl} - \gamma_i \boldsymbol{\alpha}_i \dot{\bar{\varepsilon}}^{pl} \quad (6)$$

where C_i and γ_i are material parameters that should be defined through cyclic loading tests. The parameter γ_i determines how fast the i th backstress saturates to a certain value. If γ_i is equal to zero, then the backstress linearly increases. For the multiple backstress evolution, Armstrong-Frederick describes each component as evolving independently; therefore, different kinematic shifts can be considered for the initial and reversal loadings. Chun (Chun et al, 2002) proposed the ANK model which captures the permanent softening in the cyclic loading by evolving the second backstress as

$$\dot{\boldsymbol{\alpha}}_1 = \frac{C_1}{\sigma^0}(\boldsymbol{\sigma}-\boldsymbol{\alpha})\dot{\bar{\varepsilon}}^{pl} - \gamma_1 \boldsymbol{\alpha}_1 \dot{\bar{\varepsilon}}^{pl} \quad (7)$$

$$\dot{\boldsymbol{\alpha}}_2 = \begin{cases} \dfrac{C_2}{\sigma^0}(\boldsymbol{\sigma}-\boldsymbol{\alpha})\dot{\bar{\varepsilon}}^{pl} - \gamma_2 \boldsymbol{\alpha}_2 \dot{\bar{\varepsilon}}^{pl} & \text{for initial loading} \\ 0 & \text{for reversal loading} \end{cases} \quad (8)$$

The second backstress is evolving with respect to the loading path history. The evolution of the second backstress is then considered as a function of the angle between the previous and current loading paths. In order to determine the loading direction, the strain increment direction is monitored by measuring the angle between the previous loading and current loading (Choi et al, 2006)

$$\varphi = \cos^{-1}\left(\frac{\boldsymbol{\varepsilon}_p \cdot \boldsymbol{\varepsilon}_p^*}{|\boldsymbol{\varepsilon}_p|\,|\boldsymbol{\varepsilon}_p^*|}\right) \quad (9)$$

where $\boldsymbol{\varepsilon}_p$ is for the current loading and $\boldsymbol{\varepsilon}_p^*$ is for the previous loading. If $\varphi > 90^o$, then it is considered to be in the reverse direction.

The isotropic expansion of yield surface in this Chaboche model is described by

$$\sigma_t = \sigma_0 + R_{ANK} + \alpha \ . \quad (10)$$

where σ_0 is the yield stress when $\bar{\varepsilon}^{pl}$ (the equivalent plastic strain) is zero.

The isotropic hardening part of ANK model can be written as,

$$R = R_{ANK} = K\left(1-e^{-N\bar{\varepsilon}^{pl}}\right) - \frac{C_1}{\gamma}\left(1-e^{-\gamma\bar{\varepsilon}^{pl}}\right) - C_2\bar{\varepsilon}^{pl} \qquad \text{with} \qquad \frac{C_1}{\gamma} - \alpha_1 \geq 0 \tag{11}$$

R describes the change of yield surface size from the initial yield and K, N are curve fitting parameters and α_1 is a scalar version of the backstress for a uniaxial loading condition. Therefore, the material parameters to be determined are C_1 and γ_1. In this study, we modified the ANK model to turn the second backstress to zero for the reverse loading, and it fits better to the high-strength steel. These models have been tested by using VUSDFLD and corresponding field variable that is monitoring the loading direction to turn off the second backstress when the reversal loading is detected.

3.4 Calibration of material model parameters using Isight

In this study, a program for calibrating Chaboche material model parameters was developed, which can be used i) to extract plastic strain-stress data from test results and graphically compare with results generated by selected Chaboche model using material parameters inputted into GUI directly; ii) to calibrate material parameters of Chaboche model by using an predefined Isight workflow for Half cycle model and full cycle models (ZANG and modified ANK) respectively; iii) and to perform confirmation analysis by updating material parameters in a template Abaqus model and submit it with an user-subroutine to reproduce the Bauschinger effect in analysis.

Figure 10. A Java program for fitting material parameters of Chaboche models

When button [Fitting (Isight)] on the program is pressed, a workflow shown in Figure 11 will be performed and the values of the material parameter fields will be updated with the fitted values automatically. The workflow consists of two branch processes for fitting parameters for half cycle and full cycle models separately. To improve the performance of the calibration processes, each process is separated into two phases for fitting isotropic and kinematic hardening components separately. The material parameters fitted will be written into a text file using Data Exchange component for later use.

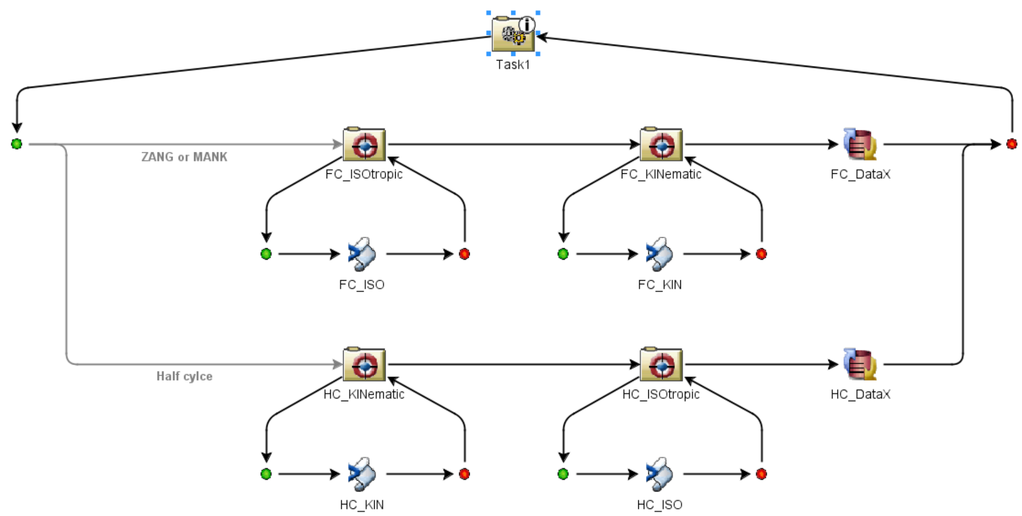

Figure 11. Workflow for fitting material model parameters

4. FEA results taking the Bauschinger effect into account

4.1 Axial crush calculation with the Bauschinger effect

Figure 12 shows the force-stroke curves and energy absorption curves of hat section frame and hexagonal section frame with 590MPa and 780MPa grades. In this simulation, Chaboche one back stress parameters obtained by Isight-Abaqus system were applied. When considering the Bauschinger effect, it was found that the accuracy of the energy absorption was greatly improved.

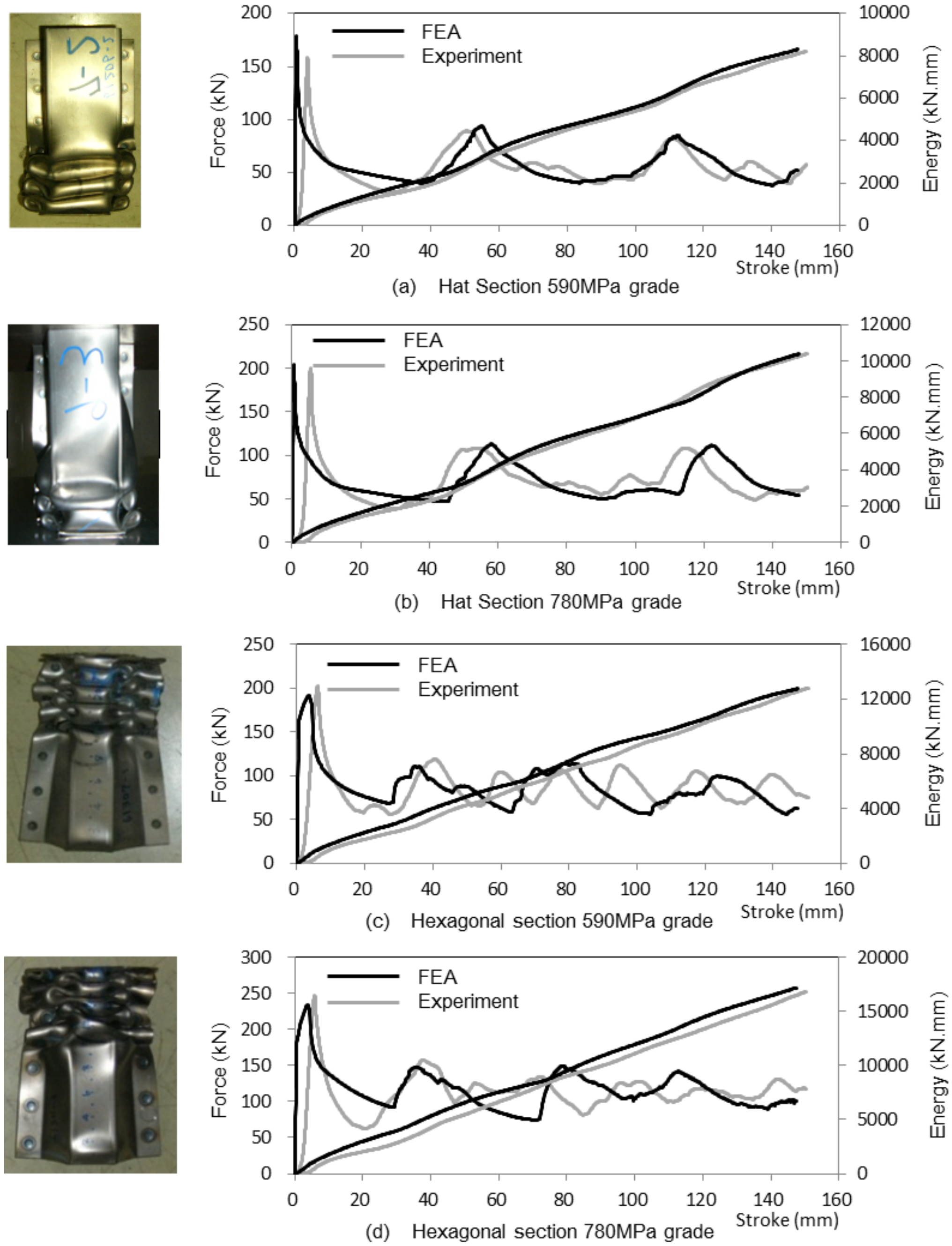

Figure 12. Force-stroke and energy-stroke curves with the Bauschinger effect

4.2 Three-point bending simulation with the Bauschinger effect

To investigate the Bauschinger effect, three-point bending tests were performed as shown in Figure 13 (Takada, Sato and Ma, 2015). The hat-section of a 70mm x 78mm, with 20mm in the flange width and 1.6mm in the thickness was used. The steel grade of hat-section was 590MPa. The angles of the left corner and the right corner were 98 degrees and 102 degrees, respectively. The hat section was assembled with a back plate with a 980MPa grade and a thickness t=1.6mm. The radius of the punch was 112mm and the radius of the support cylinders was 12.5mm. The friction factor between the back plate and the support cylinders was about 0.15. The span of the beam between the two supported points was 700mm. The punch was lowered with a constant velocity of 100mm/min. Figure 14 shows the FEA model of a three-point bending frame. In this three-point bending simulation, Chaboche one back stress parameters obtained by Isight-Abaqus system were applied.

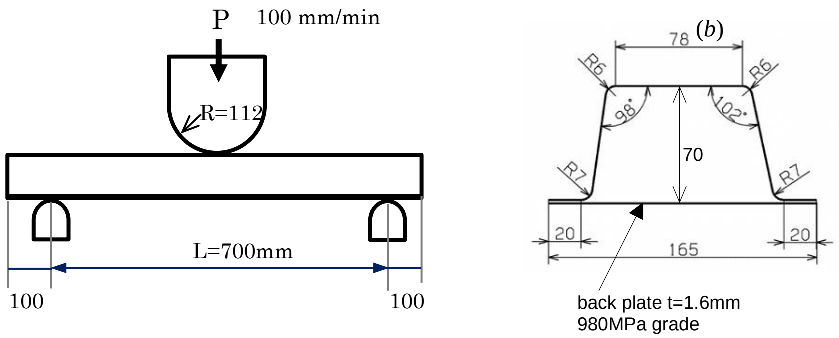

Figure 13. Dimensions of three-point bending model

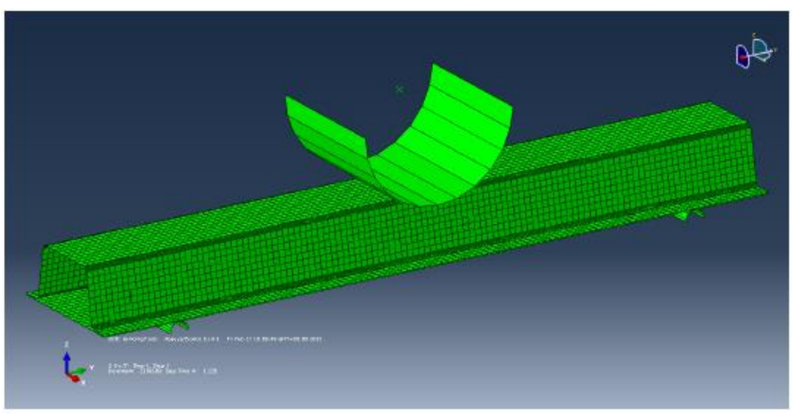

Figure 14. FEA model of three-point bending model

4.2.1 Determination of mesh pitch

In this three-point bending simulation, the mesh pitch of 4-node shell element was decided based on the Equation (12) (Wierzbicki, Recke, Abramowicz and Gholami, 1994).

$$H = 1.276 \cdot t^{1/3} b^{2/3} \tag{12}$$

In this case, it is also assumed that the total number of divisions to predict the plastic folding wave accurately is 7 or 8. According the equation (14), the length of plastic wave *2*H of this frame is 54.5mm. Consequently, the mesh pitch of this frame use the 7.76mm.

4.2.2 FEA results

Figure 15 shows the force-stroke curve of the experiment result, the FEA results with and without the Bauschinger effect, respectively. When considering the Bauschinger effect, it was found that the accuracy of force-stroke curve was greatly improved.

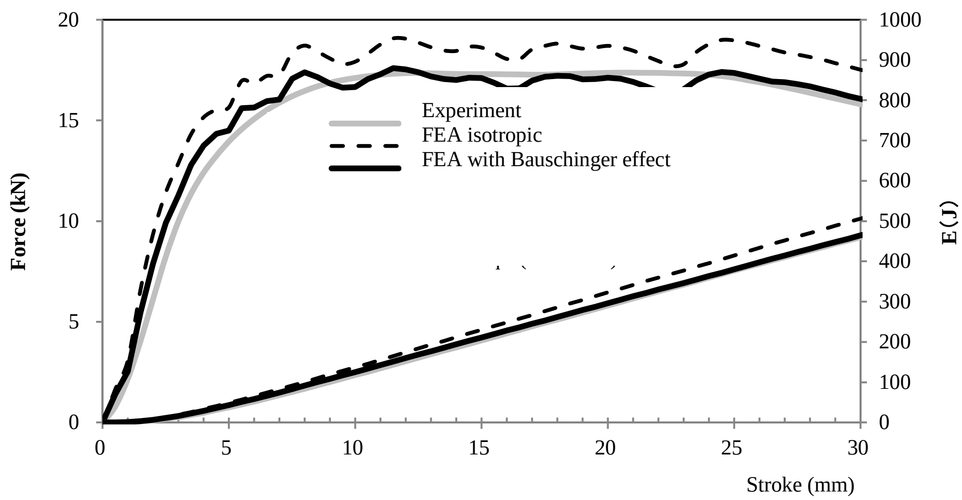

Figure 15. Comparison of force-stroke curves between the experiment and FEA results

5. Modified ANK model

In this study, it was found that Chaboche one back stress model was efficient to improve the energy absorption of hat section and hexagonal section frames. In the crash problem, most important point is to identify the compression state accurately. In other words, stress-strain curves of FEA should to reproduce the first tensile curve and next compression curve only with high accuracy, which is half cycle of tensile and compression curve. However, in the case of stamping simulation, FEA have to reproduce the full cycle curve of tensile and compression curve. In this case, modified ANK model will be very efficient to produce the full cycle curve. Figure 16 shows the identified results for standard high- strength steels.

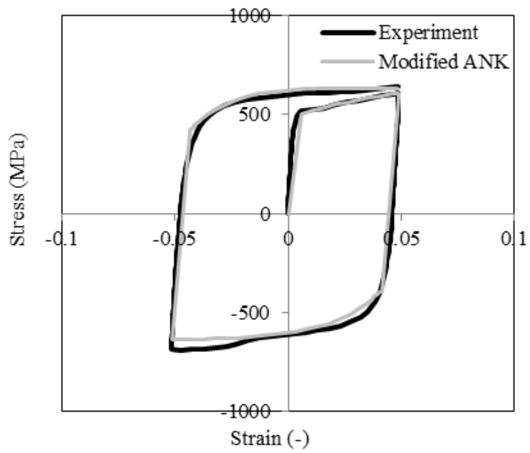

(a) 590MPa

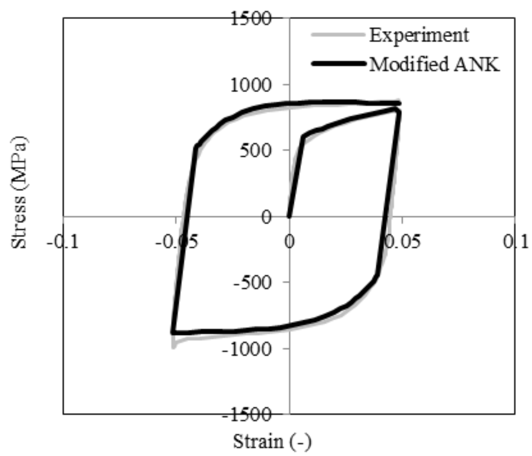

(b) 780MPa

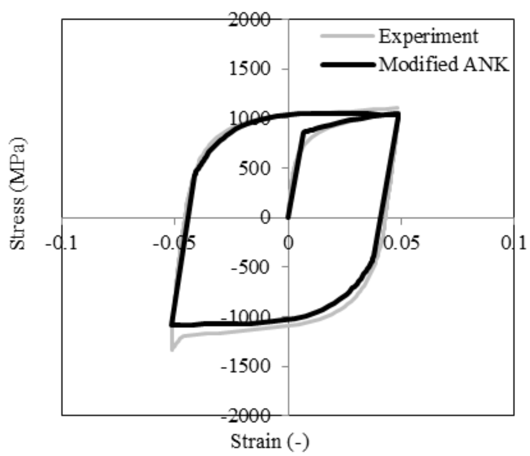

(c) 980MPa

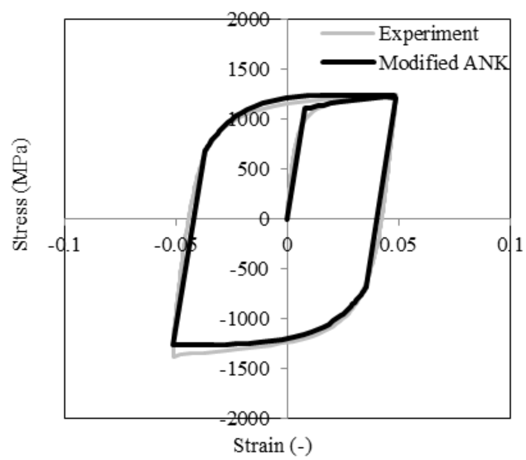

(d) 1180MPa

Figure 16. The identified results for standard high- strength steels with modified ANK model.

6. Conclusions

From this study, the following conclusions can be drawn:

The Bauschinger effect parameters of Chaboche one back stress model and modified ANK model were identified efficiently by using the Isight-Abaqus calibration program.

In the case of energy absorption of axial crash problem, it was found that by using Chaboche one back stress model, the energy absorptions of hat section frame and hexagonal section frame with high-tension steels were improved accurately.

Three-point bending test and simulation supposing an actual automobile structure were performed. By using Chaboche one back stress model, it was found that the energy absorption was accurately improved.

The tensile and compression tests were performed to measure the Bauschinger effect parameters for standard high-strength steels. By using the modified ANK model based on Isight-Abaqus calibration program, it was found that program results correlated well with the tensile and compression tests. It will be supposed that this system is useful for future stamping simulation.

7. Acknowledgments

The authors would like to thank the late Dr. W. Abramowicz of the Impact Design Europe for his valuable comments.

8. Reference

1. Armstrong, P.,J., Frederick, C.O., “A Mathematical Representation of the Multiaxial Bauschinger Effect,” G.E.G.B. Report RD/B/N 731, 1966
2. Chaboche, J.L., “Time independent constitutive theories for cyclic plasticity,” International Journal of Plasticity 2 (2), 149, 1986
3. Chaboche, J.L., “Constitutive equations for cyclic plasticity and cyclic viscoplasticity,” International Journal of Plasticity 5, pp.247-302, 1989
4. Choi, Y., Han, C.-S., Lee, J.K., Wagoner, R.H., “Modeling multi-axial deformation of planar anisotropic elasto-plastic materials, part I: Theory,” International Journal of Plasticity 22, pp. 1745-1764, 2006

5. Chun, B.K., Jinn, J.T., Lee, J.K., “Modeling the Bauschinger effect for sheet metals, part I: theory,” International Journal of Plasticity 18, 571-595, 2002
6. Datsko, J., “Material Properties and Manufacturing Processes,” John Wiley & Songs, New York, pp. 13-40, 1966.
7. Takada, K., Sato, K. and Ma, N., “Fracture Prediction for Automotive Bodies using a Ductile Fracture Criterion and a Strain-Dependent Anisotropy Model,” SAE Paper 2015-01-0567, 2015.
8. Wierzbicki, T., Recke, L., Abramowicz, W., and Gholami, T., “Stress profiles in thin-walled prismatic columns subjected to crush loading-Π. Bending,” Computer & Structures, 51(6):pp. 624-640, 1994.
9. Wierzbicki, T., Recke, L., Abramowicz, W., and Gholami, T., “Stress profiles in thin-walled prismatic columns subjected to crush loading-I. Compresion,” Computer & Structures, 51(6):pp. 611-623, 1994.
10. Wierzbicki, T. and Abramowicz, W., “The Mechanics of Deep Plastic Collapse of Thin Walled Structures Chapter 9” In Structure Failure. Wierzbicki and Jones (Editors). Wiley, New York,1989.
11. Zang, S.-L., Lee, M.-G., Kim, J.H., “Evaluating the significance of hardening behavior and unloading modulus under strain reversal in sheet springback prediction,” International Journal of Plasticity 77, 194-204, 2013

Contact Information

Kenji Takada, Chief Engineer
Honda R&D Co., Ltd. Automobile R&D Center 4630 Shimotakanezawa, Haga-machi, Haga-gun, Tochigi, Japan, 321-3393 Kenji_Takada@n.t.rd.honda.co.jp +81-80-9150-1451